Anomalous effective strain-optic constants of nonparaxial optical fiber modes

Valérie Voisin,[1,*] Christophe Caucheteur,[1] Patrice Mégret,[1] and Jacques Albert[2]

[1]*Electromagnetism and Telecom Unit, Université de Mons, 31 Boulevard Dolez, Mons, 7000, Belgium*

[2]*Department of Electronics, Carleton University, 1125 Colonel By Drive, Ottawa, Ontario K1S 5B6, Canada*

**Corresponding author: valerie.voisin@umons.ac.be*

Received November 8, 2013; revised December 19, 2013; accepted December 21, 2013;
posted January 2, 2014 (Doc. ID 201043); published January 27, 2014

We demonstrate that the experimental strain-optic coefficients for strong guided modes are not consistent with the accepted photoelastic theory. It is shown that for modes with significant nonparaxial components, such as modes guided by strong refractive index differences or in waveguides with dimensions that are much larger than the wavelengths used, the photoelastic theory should be modified to include the effect of the longitudinal components of the electromagnetic fields of the modes. Moreover, we highlight that the strain-optics coefficients depend on the state of polarization of the mode and provide a formula to calculate the necessary corrections. © 2014 Optical Society of America

OCIS codes: (060.2430) Fibers, single-mode; (230.7370) Waveguides; (060.2400) Fiber properties; (070.2580) Paraxial wave optics; (060.3735) Fiber Bragg gratings; (260.5430) Polarization.
http://dx.doi.org/10.1364/OL.39.000578

By definition, single-mode optical waveguides (and fibers, used here interchangeably) allow only one electromagnetic mode to propagate along the waveguide axis. Such waveguides are usually weakly guiding, which means that the core-cladding refractive index difference is small enough for the electric and magnetic fields of the waveguide mode to be polarized essentially transversely to the waveguide axis. Furthermore, in single-mode waveguides with complete cylindrical symmetry (optical fibers), modes of all polarizations are degenerate (i.e., they have the same electromagnetic fields, apart from rotation around the waveguide axis, and the same phase and group velocities). In recent years, strongly guided structures for modes with non-negligible axial electric fields have been increasingly used. Examples include optical nanowires for sensing or increased nonlinearity, or the large variety of cladding guiding devices for sensing applications (including long period gratings, tilted fiber Bragg gratings (TFBGs), and fiber multimode interference devices) [1–3]. Given that these devices can be used to measure strain or might suffer from strain cross sensitivity, a detailed investigation of the strain-optic constants of nonparaxial guided modes is necessary.

The purpose of this Letter is to demonstrate that the conventional theory for the effect of uniaxial strain on the optical properties of waveguide modes does not apply to strongly guided modes with non-negligibly axial components of their electric and magnetic fields (or nonparaxial modes). The test case for our model is a strained standard telecommunication optical fiber. Instead of the weakly guided light in the core, we use a TFBG [3,4] to excite nonparaxial modes guided by the glass–air interface of the fiber cladding. TFBGs are introduced in the fiber core by a photosensitive process that gives rise to a refractive index modulation with grating planes blazed by a certain angle with respect to the fiber axis, as shown in Fig. 1. The transmission spectrum of TFBGs exhibits several tens of resonances at different wavelengths. The peak resonance labeled λ_B is the result of the coupling between the co- and contrapropagating core modes. The other resonances arise from the coupling between the core mode and a contrapropagating cladding mode of the fiber [5]. The key here is that those resonances provide high-resolution probes of the mode phase velocities for a wide range of mode parameters (including field distributions and polarizations). In particular, it was reported [6] that the core and cladding mode resonances of a TFBG shift differentially in response to axial strain and that the sensitivity to strain decreases with the cladding mode order. We now proceed to show that unlike what was reported in [6] (mainly because these prior measurements did not cover a wide enough range of modes and were carried out using unpolarized light), this differential response is not consistent with the accepted photoelastic theory of optical fibers.

The wavelengths at which the discrete coupling between the jth cladding mode occurs λ^j_{clad} are given by [5]

$$\lambda^j_{\text{clad}} = (n_{\text{eff,core}} + n^j_{\text{eff,clad}})\Lambda, \tag{1}$$

where $n_{\text{eff,core}}$ and $n^j_{\text{eff,clad}}$ are, respectively, the effective refractive index of the core and of the jth cladding mode at λ^j_{clad} and $\Lambda_G = \Lambda \cos\theta$, with Λ the periodicity of the

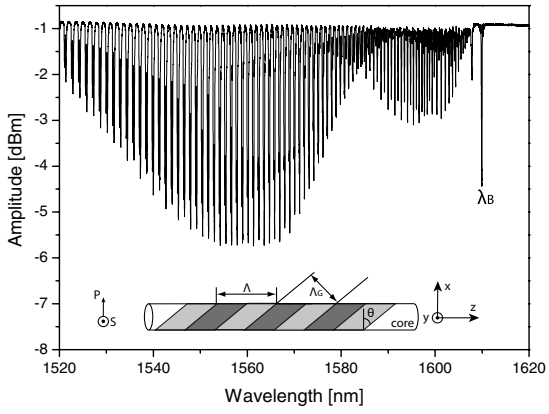

Fig. 1. Transmission spectrum of a 10° TFBG measured in air and used for experiments and sketch of the light coupling mechanism for TFBGs.

index variation and θ the tilt angle of the grating planes. The effective indices are related to the phase velocities of the guided modes by $v_p = c/n_{\text{eff}}$. When mechanical strain is applied on the fiber, the resonance wavelengths shift because of changes in both the effective index of the modes and the periodicity of the grating. The wavelength shift $\Delta\lambda^j_{\text{clad}}$ caused by an axial strain variation (Δs) can be derived from Eq. (1) as [6,7]

$$\Delta\lambda^j_{\text{clad}} = \lambda^j_{\text{clad}}(1 - p^j_{\text{clad}})\Delta s, \tag{2}$$

where p^j_{clad} is the effective strain-optic coefficient for the jth cladding mode. This coefficient is

$$p^j_{\text{clad}} = \frac{-1}{(n_{\text{eff,core}} + n^j_{\text{eff,clad}})} \frac{\partial(n_{\text{eff,core}} + n^j_{\text{eff,clad}})}{\partial s}. \tag{3}$$

The effect of axial strain on the effective index comes from the refractive index variation due to the photoelastic effect and the change in diameter (D) of the optical fiber. Therefore, $\partial n^j_{\text{eff,clad}}/\partial s$ can be expressed as

$$\frac{\partial n^j_{\text{eff,clad}}}{\partial s} = \frac{\partial n^j_{\text{eff,clad}}}{\partial n}\frac{\partial n}{\partial s} + \frac{\partial n^j_{\text{eff,clad}}}{\partial D}\frac{\partial D}{\partial s}. \tag{4}$$

This is where the conventional photoelastic theory of optical fiber modes starts to become restricted to weakly guided, essentially transverse optical modes, because $\partial n/\partial s$ is taken to be the variation of the component of the refractive index tensor that lies in the direction transverse to the waveguide axis (or z axis, along which the strain is applied). The second term in Eq. (4) represents the effect of the change in waveguide dimensions due to axial strain, given by $\Delta D = \nu s D$ where ν is Poisson ratio (0.16) [8]. The photoelastic term $\partial n/\partial s$, for the variation of refractive index along the transverse direction for an axial strain along z, can be calculated from [8]

$$\frac{\partial n}{\partial s} = -\frac{1}{2}n^3(p_{12} - \nu(p_{11} + p_{12})) = -0.296, \tag{5}$$

where n refers to the core or cladding refractive index ($n_{\text{core}} = 1.4499$, $n_{\text{clad}} = 1.4440$ for wavelengths near 1550 nm), and p_{11} and p_{12} are the components of the strain-optic tensor ($p_{11} = 0.11$, $p_{12} = 0.252$ for a typical single-mode fiber [SMF] [7], Corning SMF-28 in this case).

The calculation of the modal strain-optic coefficients [Eq. (3)] is carried out by simulation (using FIMMWAVE, by Photon Design). A set of effective indices is calculated for the unstrained fiber and another set for a modified fiber where the refractive indices of both core and cladding are modified according to Eq. (5) (for the strains considered here the change in effective index due to diameter change is under 10^{-5} and negligible compared with the photoelastic terms). Comparing the two mode sets provides the necessary values for $\partial n_{\text{eff}}/\partial s$. These results will be presented below in comparison with experimental values.

One-centimeter-long TFBGs manufactured into hydrogen-loaded SMFs using a 248 nm excimer pulsed laser and the phase mask technique were strained. The internal tilt angle was set to 10°. The setup used to collect the TFBG amplitude spectrum is made up of a JDSU optical vector analyzer (SWS OMNI 2 System). Different axial strain values were applied with calibrated weights (between 10 and 180 g) hung on the optical fiber. The strain was derived from the weight through the use of Hooke's law with a Young's modulus of 73 GPa for the fiber [8]. For each strain, we measure the cladding mode resonance wavelengths, with a repeatability of ±3 pm.

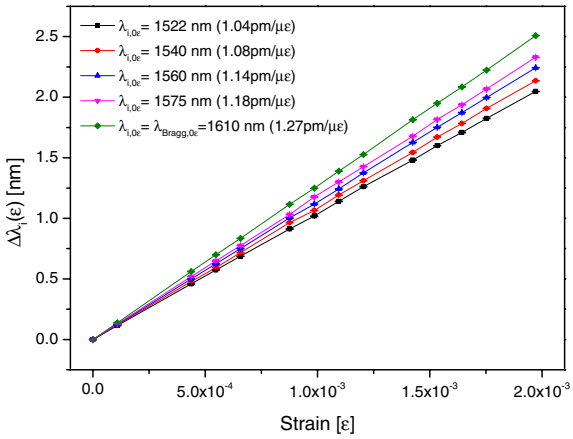

Fig. 2. Relative wavelength variations as a function of the axial strain for core mode and some cladding modes.

Figure 2 shows the relative wavelength shifts of the core and selected cladding modes with longitudinal strain (in a range 0–1970 με corresponding to 0–180 g). The relative evolutions are obtained through the difference between the data measured at a given axial strain and the reference data measured in the absence of strain. The cladding mode resonances shift differentially (with the cladding mode order) and always slightly less than the Bragg wavelength in response to axial strain. We obtain a sensitivity of 1.27 pm/με for the Bragg mode and 1.04 pm/με for the cladding mode at ~1522 nm (one of the highest-order modes that we are able to record in the amplitude spectrum). A further refinement of the measurement takes into account the fact that high-order cladding modes come in nearly degenerate pairs composed from two polarized mode families: each mode pair is made up of one azimuthal (HE_{mn} or TE_{0n}) and radial (EH_{mn} or TM_{0n}) mode [3]. Input light linearly polarized in the plane of the tilt (P-polarization) couples to radially polarized modes, while light polarized perpendicularly to it (S-polarization) couples to azimuthal modes. The swept wavelength system provides the individual S- and P-polarized spectra. We then observe distinctly both resonances that compose each cladding mode pair in the amplitude spectrum so as to measure the impact of the axial strain as a function of the state of polarization (SOP) and mode order. Figure 3 depicts a zoom around a pair of high-order cladding mode resonances for two different axial strain states, at 0 and 1970 με.

Figure 4 compares the strain sensitivity ($\Delta\lambda_j/\Delta s$) for a cladding mode pair with resonance wavelengths near 1522 nm and demonstrates that the radial mode resonance lags behind that of the azimuthal mode. For the cladding modes around 1522 nm, the sensitivity is 1.02 pm/με for the azimuthally polarized mode and

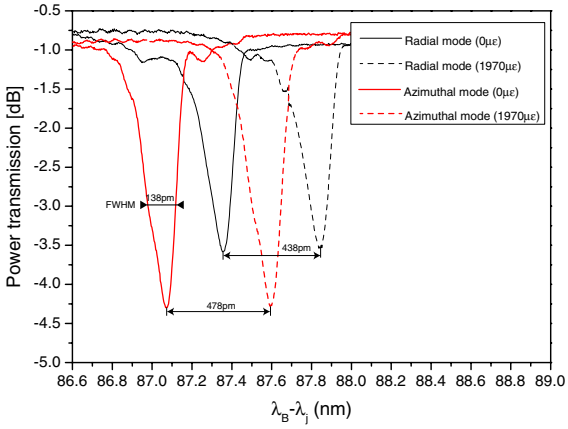

Fig. 3. Zoom on a pair of resonances located 87 nm away from the Bragg wavelength for two axial strain values.

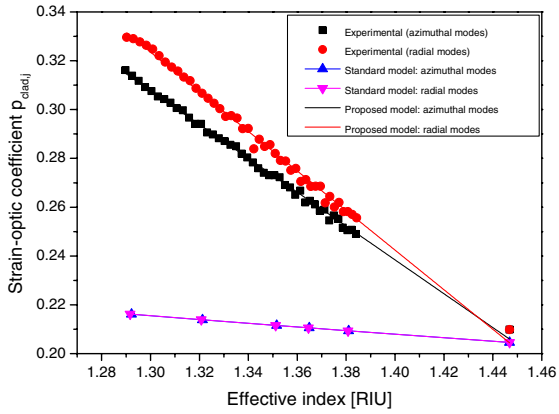

Fig. 5. Comparison of experimental and simulated p_{core} and p_{clad} (between 1522 and 1575 nm).

1.04 pm/με for the radially polarized mode. The difference of the wavelength variation for radial and azimuthal modes increases linearly with strain. Figure 5 shows experimental results expressed in terms of strain-optic coefficients of all the modes considered. The mode spacing at wavelengths shorter than 1575 nm calculated from data by Eq. (2) becomes too small to effectively extract accurate mode resonance wavelengths, but there is a clear linear trend in the strain-optic coefficients all the way from the core mode to the highest-order cladding modes that we could measure, as well as a very significant difference between the two mode families that is also increasing linearly. From these experimental results, we can deduce that the strain-optic coefficients p^j_{clad} increase with mode order and are higher for radially polarized modes than for azimuthally polarized modes. Figure 5 compares the values of experimental and exact analytical strain-optic coefficients [Eqs. (3)–(5)]. It is clear that while the model describes the core mode coefficient accurately, it fails by increasingly large amounts for higher-order modes. Indeed, the difference between theoretical and experimental values for the core mode is about 3%, while it reaches 50% for the cladding mode at 1520 nm. This clearly indicates that the accepted theory does not take into account some physical effect related to cladding modes only. An error in the evaluation of the strain can be ruled out because our result and theory for the core mode are consistent with the accepted value for this kind of fiber, that is, near 0.22 [7].

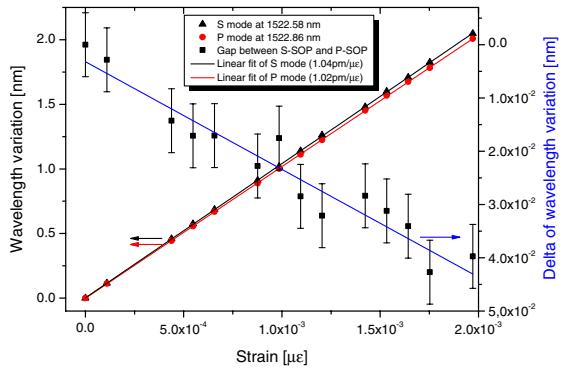

Fig. 4. Wavelength variation as a function of axial strain for S and P (SOP) and delta of wavelength of variation.

We postulate that the nonparaxiality of the cladding modes can explain this difference. In recent years the contribution of longitudinal field components in strongly guiding structures (such as optical fiber and silicon waveguide microwires) has been brought forward to explain some experimental discrepancies in nonlinear optic phenomena [9]. The cladding of a fiber in air certainly qualifies as a strongly guiding structure, and cladding modes of increasing order have correspondingly increasing longitudinal (z) field components.

Over the range of modes studied here, the equivalent angle of inclination of the mode ray vectors relative to the fiber axis varies linearly from 3° to 27°, and from the electromagnetic theory point of view, the main consequence of nonparaxial propagation is that the mode fields are not transverse (i.e., confined to the x–y plane), as is the case for weakly guiding structures (such as the core-cladding system). Therefore, in addition to Eq. (5), which expresses the effect of the longitudinal strain on the x and y components of the refractive index, the photoelastic factors in Eq. (4) must be modified to include the effect of the strain on n_z, the refractive index for the fraction of the light with an electric field vector polarized along z [8]:

$$\frac{\partial n_z}{\partial s} = \frac{-n_z^3}{2}(p_{11} - 2\nu p_{12}) = -0.044. \tag{6}$$

This additional term will impact only radial modes, that is, the only ones with an E_z component, and increase p_{clad} for these modes. This contribution cannot solely account for the large increase in the photoelastic coefficients because it is equal to zero for azimuthal modes but is likely the source of the difference between the radial and azimuthal p_{clad} values observed experimentally. Quantitatively, the contribution of nontransverse fields can be accounted for by using the following formula [10]:

$$n_{eff} = \frac{c}{P}(W_T - W_Z), \tag{7}$$

$$\frac{\partial n_{eff}}{\partial s} = \frac{c}{P}\left(\frac{\partial W_T}{\partial s} - \frac{\partial W_Z}{\partial s}\right), \tag{8}$$

where W_T and W_Z are the total transverse and longitudinal energy densities per unit length, P is the magnitude of the Poynting vector, and c the speed of light in vacuum. W_T and W_Z are, respectively, defined by

$$W_T = \iint \left[\frac{1}{2}\epsilon_0 n_x^2 E_T^2 + \frac{1}{2}\mu_0 H_T^2\right] \mathrm{d}x\mathrm{d}y, \tag{9}$$

$$W_Z = \iint \left[\frac{1}{2}\epsilon_0 n_Z^2 E_Z^2 + \frac{1}{2}\mu_0 H_Z^2\right] \mathrm{d}x\mathrm{d}y, \tag{10}$$

where ϵ_0 and μ_0 are the permittivity and permeability in vacuum. $E_{T(Z)}$ and $H_{T(Z)}$ define the transverse and longitudinal components of the electric and magnetic fields.

It turns out that W_T and W_Z both change linearly with effective index over the range studied: a contribution from the axial energy density has the correct sign and order (linear) to explain the experimental observations. The difference between radial and azimuthal modes can be further explained by the fact that for radial modes the axial energy density is entirely due to electric fields (W_Z^E), while for azimuthal modes the axial energy is magnetic (W_Z^H). Therefore we propose the following expression to replace Eq. (4):

$$\frac{\partial n_{\mathrm{eff}}}{\partial s} = \frac{c}{P}\left(\frac{2}{n_x} W_T^E \frac{\partial n_x}{\partial s} - a W_Z^E - b W_Z^H\right), \tag{11}$$

where the first term on the right-hand side corresponds to the standard photoelastic formulation [it is equivalent to Eq. (4)] and the next two terms to the contributions of the axial fields. The model represented by Eq. (11) is used instead of Eq. (4) and plotted on Fig. 4, using $a = 2.05$ and $b = 1.40$ with mode energy densities calculated from Eqs. (9) and (10).

In conclusion, the effective strain-optic constants of the cladding modes of standard SMF were measured and found to be in strong disagreement with the accepted model based on photoelasticity theory. While this model correctly predicts the effect of strain on the effective index and polarization of the weakly guided core mode, the results presented here clearly show that for cladding modes of increasing order, the theory and measurement diverge linearly with mode effective index, reaching a difference of 50% for modes with effective indices near 1.3 (i.e., strain-optic coefficients of 0.32 [TE-HE] and 0.33 [TM-EH] instead of 0.206). These results are consistent with a hypothesis where the effect of axial strain on the permittivity tensor of the fiber and its subsequent coupling to the mode effective indices is linearly dependent on the axial components of the mode profiles for strains between 0 and 2000 με and mode effective indices between 1.3 and 1.45. An empirical model is proposed to improve the calculation of the photoelastic coefficients by including terms dependent on the axial mode field components.

This work is supported by the European Research Council (ERC) through the Starting Independent Researcher Grant PROSPER, the F.R.S.-FNRS, NSERC, and the Canada Research Chairs program.

References

1. S. W. James and R. P. Tatam, Meas. Sci. Technol. **14**, R49 (2003).
2. G. Brambilla, F. Xu, P. Horak, Y. Jung, F. Koizumi, N. P. Sessions, E. Koukharenko, X. Feng, G. S. Murugan, J. S. Wilkinson, and D. J. Richardson, Adv. Opt. Photon. **1**, 107 (2009).
3. J. Albert, L.-Y. Shao, and C. Caucheteur, Laser Photonics Rev. **7**, 83 (2013).
4. T. Erdogan and J. E. Sipe, J. Opt. Soc. Am. A **13**, 296 (1996).
5. G. Laffont and P. Ferdinand, Meas. Sci. Technol. **12**, 765 (2001).
6. C. Chen and J. Albert, Electron. Lett. **42**, 1027 (2006).
7. A. Othonos and K. Kalli, *Fiber Bragg Gratings* (Artech House, 1999).
8. C. D. Butter and G. B. Hocker, Appl. Opt. **17**, 2867 (1978).
9. S. Afshar and T. M. Monro, Opt. Express **17**, 2298 (2009).
10. H. Kogelnik, in *Integrated Optics*, T. Tamir, ed. (Springer-Verlag, 1979).